INVITED REVIEW

A brief review of actuation at the micro-scale using electrostatics, electromagnetics and piezoelectric ultrasonics

Daniel Kuang-Chen Liu, James Friend* and Leslie Yeo

*MicroNanophysics Research Laboratory,
Department of Mechanical and Aerospace Engineering,
Monash University, Melbourne Australia 3800*

Abstract: Though miniaturization and mass production via integrated circuit fabrication techniques have transformed our society, the methods have yet to be successfully applied to the generation of motion, and as a consequence the many potential benefits of microrobotics has yet to be realized. The characteristics of electrostatic, electromagnetic and piezoelectric transduction for generating motion at the micro scale is considered, employing scaling laws and a reasoned consideration of the difficulties in motor fabrication and design using each method. The scaling analyses show that electrostatic, electromagnetic and piezoelectric actuators all have comparable force scaling characteristics of $F \propto L^2$; if one employs *permanent* magnets, electromagnetic forces do not scale as $F \propto L^4$. Though the torque, τ, of piezoelectric ultrasonic motors scale rather poorly with $\tau \propto L^4$, they have the clear advantage of possessing torque amplitudes some two orders of magnitude larger than motors employing the other transduction schemes at the micro scale.

1. INTRODUCTION

Miniaturization has been important to many of the technological advances that have occurred in the past fifty years. Since the invention of the integrated circuit in the 1950s, continual improvements in microfabrication techniques have enabled an exponential decrease in the size of microelectronic components [1]. The ever greater diversity, economy and power of these electronic components have enabled personal computers, laptops, digital cameras, and mobile phones, paving the way for the information technology revolution that has transformed our society [2].

The overwhelming success of miniaturization in electronics has inspired efforts to miniaturize systems from other fields. A major goal in the research of miniaturization technologies is the creation of autonomous miniature machines or micro-robots that can perform useful tasks under severe space constraints [3]. Some of the technologies needed for the development of micro-robots such as sensors [4] and controllers [5,6] are already available at the sub-millimeter scale, however, significant progress is still needed in actuation, power, and control strategies. Here, we focus upon the challenge of *actuating* sub-millimeter scale micro-robots.

*e-mail: James.Friend@eng.monash.edu.au
 URL: http://mnrl.monash.edu

2. COMPARISON OF SMALL MOTOR TECHNOLOGIES

Researchers have investigated many different actuation methods for micromotors, utilizing a diverse range of phenomena from electrostatic and magnetic to piezoelectric effects. In this section we will examine the characteristics of the above mentioned motor technologies, describing their working principles, scaling laws, current level of performance, and potential for further improvements.

2.1. Electrostatic Motors
2.1.1. Scaling of electrostatic forces
The basic motive force employed in electrostatic actuators arises from the electrostatic interaction between electric charges. A simple example of such an actuator is the parallel plate capacitor (see Fig. 1). For a constant voltage of V, the potential energy U stored in the capacitor as a function of the parallel x and normal and plate z displacements is $U(x,z) = -\frac{1}{2}C(x,z)V^2$, with $C(x,z) = \epsilon\frac{(L_x-x)L_y}{z}$, where C is the capacitance, L_x and L_y are the plate dimensions, ϵ is the permittivity of the dielectric layer, and the effect of fringing fields is neglected. The tangential F_x and normal F_z forces tending to realign the plates due to the relative displacements are
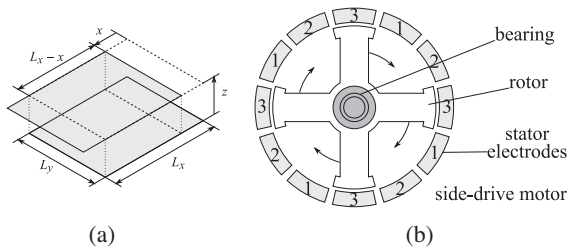
Fig. 1 Illustrations of (a) a typical parallel-plate capacitor and (b) a three-phase, electrostatic side-drive motor [7].

Fig. 2 Different types of electrostatic motors: (a)–(b) cross-section side view of side-drive and top-drive motors, (c) top view of the wobble motor, and (d) the schematic diagram of the operation of an electrostatic induction motor.

$$F_x = -\frac{\partial U}{\partial x} = -\frac{1}{2}\epsilon L_y z |E|^2, \quad \text{and} \quad F_z = -\frac{1}{2}\epsilon L_x L_y |E|^2, \tag{1}$$

where the electric field $|E| = V/z$ is limited to $|E| < |E_b|$, the breakdown electric field of the dielectric layer. Since the permittivity ϵ is a scale independent property, and the scaling law (in terms of linear scale variable L) for the breakdown field E_b is known to lie between $L^{-0.5}$ and L^0 [8,9] (increasing slightly as scale is decreased), the force scaling law for electrostatic actuators is estimated from Eq. (1) to be between L^1 and L^2.

2.1.2. Motor designs

Although parallel plate actuators have limited stroke lengths, they can be used to generate continuous rotary motion by a proper manipulation of charge distributions on a set of stationary electrodes (stator) and free moving electrodes (rotor). Since research on the creation of MEMS micromotors using silicon-based microfabrication techniques began in the 1980s, a number of electrostatic motor designs have been demonstrated [7,10]. The reported designs can be broadly classified as variable-capacitance motors, or electrostatic induction motors [11–13]. Variable-capacitance motors were the earliest successful MEMS electrostatic micromotors. The torque generated by the motor is proportional to the rate of change in the stator-rotor capacitance as a function of rotor position [3,11]. Three types of variable-capacitance motors that has been reported are: (1) the top-drive motor, where tangential driving forces are developed between the overlapping electrodes on the planar faces of the stator and rotor, (2) the side-drive motor, where tangential driving forces arise from the electrodes on the stator-rotor sidewalls, and (3) the harmonic side-drive or wobble motor, where the rotor rolls along the insulated sidewall of the stator and the motive torque arises from electrostatic forces between the stator and the rotor about the contact point.

Due to its larger variable capacitance, top-drive motors have the potential to provide larger motive torque than side-drive motors. However, initial research on top-drive motors found that the design suffers from rotor instability
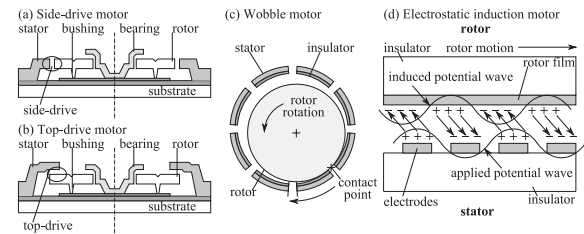
due to the presence of vertical forces that tend to clamp the rotor to the stator or the substrate [14]. Subsequently, focus was placed on side-drive motors, sacrificing output torque for rotor stability. Side-drive motors with diameters of the order of $100\,\mu m$ operated at high speeds and low torques of up to $15,000\,rpm$ and $10\,pNm$.

Attempts to overcome the low torque output of side-drive motors lead to the design of harmonic side-drive motors with built-in speed reduction mechanism that amplified the output torque. Reduction ratios of up to 200 [15] and outputs of the order of $200\,nNm$ at $300\,rpm$ and stator diameter of $560\,\mu m$ [10] have been reported. Recently, researchers have overcome some of the difficulties with top-drive motors through the use of microball bearings. The reported motor has a diameter of $14\,mm$, with a maximum power of $307\,\mu W$, torque of $5.6\,\mu Nm$ and speeds of $517\,rpm$ [16].

Electrostatic induction motors have been investigated analytically in the late 1980s as an alternative design to variable-capacitance micromotors [17]. The basic design consists of two disks separated by an air gap: the rotor disk is coated with a film of slightly conductive material, and the stator disk is covered with an array of radial electrodes (see Fig. 2). By exciting a potential wave that travels around the stator, image charges are induced on the rotor film. The conductivity of the rotor is chosen such that the image charges lag behind the stator excitation as they conduct through the rotor film. This gives rise to tangential electric field component that pulls the image charges and results in a torque on the rotor [13]. An induction motor with a rotor diameter of $4\,mm$ has been developed by a team from Massachusetts Institute of Technology (MIT) for Power MEMS applications [12,18]. The motor is capable of generating an output torque of $3.5\,\mu Nm$ at speeds and powers in excess of $55,000\,rpm$ and $20\,mW$.

2.2. Electromagnetic Motor

2.2.1. Scaling of magnetic forces

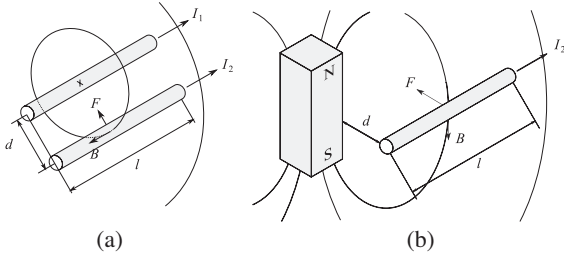There are two basic configurations for magnetic actuators (see Fig. 3), consisting of a current I_1 interacting

Fig. 3 Basic configuration of magnetic actuators: (a) current-current interaction, and (b) current-magnetic interaction.

with the magnetic field B generated by: (a) another current I_2, or (b) a permanent magnet. The magnetic field generated by current I_2 is

$$B = \frac{\mu_0}{2\pi d} I_2, \tag{2}$$

where μ_0 is the permeability and d is the radial distance from the current; on the other hand, the magnetic field generated by a permanent magnet with constant magnetization scales as L^0 when both the location and volume of the magnet are scaled. The force law for a magnetic field and a current carrying wire segment dl is $dF = Idl \times B$, which allows us to estimate the force between (a) two current carrying wires F_a, and (b) a current and a permanent magnet F_b as

$$F_a = \frac{\mu_0}{2\pi} \frac{l}{d} I_1 I_2 \quad \text{and} \quad F_b = I_2 l \times B. \tag{3}$$

Trimmer, *et al.* [9], describes three possible scaling laws for current, depending on which parameters are assumed to be intensive variables. If the maximum allowable current density J is intensive, current $I = JA$ scales as $I \propto L^2$; if the heat dissipation rate $\dot{Q}/A_s$ and the wire resistivity ρ are intensive, the balance between Joule heating $\dot{Q} = \rho \frac{l}{A} I^2$ and dissipation implies that current scales as $I \propto L^{1.5}$; if the maximum allowable temperature ΔT, wire resistivity ρ and thermal conductivity k are intensive, the balance between conductive heat dissipation and Joule heating $\dot{Q} = k \frac{\Delta T}{\Delta r} A_s = \rho \frac{l}{A} I^2$ implies that current scales as $I \propto L$. The force scaling law due to Eq. (3) and the above current scaling laws are summarized in Table 1.

2.2.2. Motor designs

There are various ways magnetic forces can be exploited to generate continuous rotary motion. Many of the motor designs have analogous electrostatic counterparts, for example, the variable magnetic reluctance motor is the counterpart of the variable capacitance motor, and the magnetic induction motor is the counterpart of the electrostatic induction motor. As with electrostatic motors, microfabrication technique constraints limit the motor to 'pancake-type' top-drive and concentric side-drive configurations.

The variable reluctance micromotors constructed to date have been side-drive motors consisting of an array of coil-wound stator poles concentric with the poles of a ferromagnetic rotor. When a pair of stator poles is energized, a force acts to align the rotor to minimize the reluctance of the stator-rotor magnetic circuit. The side-drive variable reluctance motors are among the earliest magnetic micromotors fabricated using MEMS techniques. A LIGA fabricated nickel-core motor [19] with a rotor diameter of 423 μm and thickness of 55 μm operated at speeds up to 12,000 rpm (torque was not reported); the axial component of the reluctance force was used to levitate the rotor to reduce friction, enabling it to operate for 5×10^7 revolutions without observable wear. In a different Ni-Fe-core motor of similar dimensions [20], the torque is estimated to be of the order of 3 nNm.

In a magnetic induction micromotor [21,22], a travelling magnetic wave is excited in the stator via a set of planar coils patterned arround ferromagnetic cores. The induced eddy currents in the rotor interacts with the travelling magnetic wave, resulting in a net torque and an attractive force between the stator and rotor. Two top-drive micromotors using Ni-Fe cores have recently been reported: one with a 10-mm-diameter-rotor and a stall torque of up to 2.5 μNm [22], and one with a 4-mm-diameter-rotor and a stall-torque of up to 4.8 μNm [23]. Both were fabricated and tested with a tethered rotor to avoid the complexity of designing the bearing.

The force scaling laws for magnetic actuators in Table 1 indicate that the performance of magnetic actuators benefits significantly from the use of high-strength permanent magnets. Brushless DC motors containing side-driven permanent magnet rotors are commercially available [24,25] at diameters as small as 2 mm, operating at stall torque and no-load speed of the order of 10 μNm and 10^5 rpm. Planar top-drive designs more suitable for microfabrication techniques have been demonstrated by Achotte, *et al.* [26]; with a rotor diameter of 8 mm, the motor produced an estimated torque of 100 μNm and speeds in excess of 1.4×10^5 rpm.

2.3. Piezoelectric Motor

2.3.1. Scaling of piezoelectric actuators

Unlike electrostatic and electromagnetic actuators that employ force fields acting at a distance, the force used in a

Table 1 Force scaling law of magnetic actuators.

	current-current	current-magnet
$I \propto L^2$	L^4	L^3
$I \propto L^{1.5}$	L^3	$L^{2.5}$
$I \propto L^1$	L^2	L^2

piezoelectric acutator arises from the stress and deformation experienced by piezoelectric materials due to the application of electric field witin them. The linear model of piezoelectric materials are described by the following constitutive equations [27],

$$T_{ij} = c_{ijkl}^E s_{kl} - e_{kij}E_k, \quad D_i = e_{kij}S_{kl} + \epsilon_{ij}^S E_k, \qquad (4)$$

where T is stress, S is strain, E is electric field, D is electric displacement, c is the stiffness, ϵ is the permittivity, and e is the piezoelectric coupling coefficient. The force output of piezoelectric actuators is limited by the tensile and compressive fatigue strength of the piezoelectric material, which are on the order of 0.2–0.3 MPa and 5–6 MPa respectively [28]. Assuming that the properties of piezoelectric materials are scale independent, the stress of a piezoelectric transducer scales as L^0 and thus the force scales as $F \propto L^2$. It should be noted that piezoelectric thin films generally have poor effective electromechanical coupling [27] (compare values given in [29,30]). Individually machined pieces from the bulk material give better performance, but are incompatible with batch microfabrication techniques.

2.3.2. Motor designs

Piezoelectric transducers have short stroke lengths and high resonance frequencies. In order to generate continuous rotary motion, piezoelectric motors are designed so that the frictional stator-rotor interaction rectifies the reciprocatory stator input to generate non-zero motive torque. A large number of piezoelectric motors are designed to operate at resonance frequencies to take advantage of the amplified stator motion; they are commonly referred to as ultrasonic motors because the resonance frequencies are typically in the ultrasonic range. There are non-resonant designs such as inchworm motors [31,32], however their very-high-torque-at-low-speed characteristics [56] makes them better for high holding force applications such as precision platform positioning than for the propulsion of microrobots. We will thus focus upon ultrasonic motors.

Ultrasonic motors can be classified by the type of stator motion that is used to drive the rotor. More specifically, if we describe the trajectory traced by a force transmitting point on the stator tip using a cylindrical coordinate system (r, θ, z) with z aligned with the rotor axis, the stator motion of existing motors can be divided into two categories: ellipse-like curves that lie predominantly in (1) the constant-z surface, or (2) the constant-r surface. Ultrasonic motors can be further classified according to how the different vibration modes of the stator is combined to generate the desired stator trajectory. Mode conversion motors are among the earliest designs of ultrasonic motors (Ref. [33,34] according to Ref. [28]). They use longitudinal vibrators that are held at particular angles and positions such that the stator-tip exerts a tangential force on the rotor

when they come into contact. The stator traces an elliptical trajectory due to its interaction with the rotor, which may lie on the constant-r or z surface, depending on whether the design is top or side-driven. A 30-mm diameter top-drive motor with wedge-shaped vibrator pieces was demonstrated by Sashida [28], which generates a stall torque of 0.5 Nm and no-load speed of 2,600 rpm. The wedge-type motor with single vibrator can achieve a high efficiency of up to 87%, however, it can only rotate in a single direction and has a short lifespan due to the repeated stator-rotor collision.

Travelling-wave motors use constant-r elliptical stator trajectories to drive the rotor. The stator consists of a metal ring bonded to two sets of transducers, each set consists of oppositely poled piezoelectric ceramic plates in an alternating pattern. By exciting the two sets of transducers 90° out of phase, a travelling flexural wave is set up in the stator ring such that each point on the stator traces an elliptical motion [28]. Travelling-wave motors as small as 8 mm in diameter and 3 mm in height have been demonstrated by Flynn, *et al.* [35], producing a stall torque of 1 mNm, a no-load speed of 1,710 rpm and a peak power output of 27 mW. The travelling-wave motor is difficult to fabricate at submillimeter scales due to the complex geometry of the stator teeth, dual-signal drive, and alternating poling pattern required by the transducer.

Flexural standing-wave motors generate constant-z elliptical motion by combining two orthogonal bending modes that are excited out of phase, as shown in Fig. 4(a). In axisymmetric structures with degenerate bending modes, this can be done using two perpendicular input excitations; alternatively, in structures where the two bending modes are coupled, this can be done using a single input excitation.

Examples of stators with degenerate bending modes include Morita, *et al.*'s hollow titanium cylinder (1.4 mm in diameter, 5 mm in length) with thin-film PZT deposited on the surface [36], and Kanda, *et al.*'s micro-machined bulk PZT cylinder (0.8 mm in diameter, 2.2 mm in length) with a nickel electrodes plated on the inner and outer surface [37] (see Table 2 for their performance). The design allows detailed control over the stator trajectory; the rotor's motion can be reversed by shifting the phase lag between the two inputs by 180°. However the design faces fabrication issues: the use of thin-film PZT gives poor performance, and micro-machining of bulk PZT is difficult at dimensions smaller than 1 mm [29].

Examples of stators with coupled bending vibration include Cagatay, *et al.*'s brass cylinder (1.6 mm in diameter, 6 mm in length) with PZT plates glued to two flattened sides [38,42]. Each PZT excites the stator tip to rotate in a fixed orientation, thus two inputs are needed for the reverse rotor motion. The design is simpler to fabricate
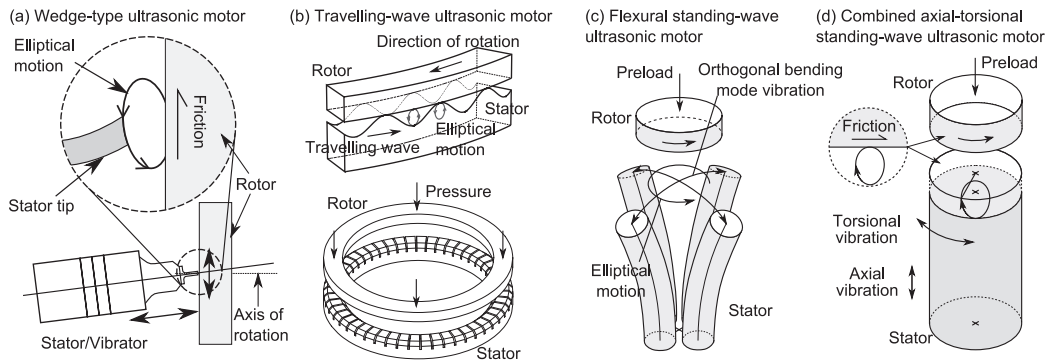
Fig. 4 Four types of piezoelectric ultrasonic motors classified by the method used to generate the desired elliptical stator trajectory.

Table 2 Performance and specification of various ultrasonic motors: mode conversion (MC), travelling-wave (T), flexural standing-wave (FS), and combined axial-torsional standing-wave motors (CATS).

Type	Motor	Diameter (mm)	Power (W)	Stall τ (Nm)	No-load speed (rpm)
MC	Sashida [28]	30	34	500 m	2,600
T	Flynn [35]	8	27 m	1 m	1,710
FS	Morita [36]	1.4	12 μ	0.67 μ	680
	Kanda [37]	0.8	2.5 μ	0.025 μ	3,850
	Cagatay [38]	1.6	45 m	500 μ	430
CATS	Satonobu [39]	20	1.5	0.8	140
	Suzuki [40]	15	10	0.22	1,100
	Watson [41]	0.25	4.3 μ	13 n	1,290

and provides better performance than the degenerate bending mode designs.

Combined axial-torsional standing-wave motors transmits motive torque to the rotor via ellipse-like stator trajectories on the constant-*r* surface. Currently there are two types of stators design for generating the combined axial and torsional motion. The first type of stator uses two separate excitation inputs: an axially-poled and a circumferentially-poled piezoelectric transducer. An example of this design is Satonobu, *et al.*'s 20 mm-diameter motor which has a maximum stall-torque and no-load speed of up to 0.8 Nm and 15 rad/s, respectively [39]. Rotor direction is easily reversed by changing the phase lag between the axial and torsional inputs, however the design is difficult to miniaturize due to the use of circumferentially-poled transducers. The second type of stator uses an axially-poled transducer and a structure with coupled axial-torsional vibration to convert the linear input into the desired stator trajectory. Examples of such designs include motors by Suzuki, *et al.* [40] and Watson, *et al.* [41], both using cylinders with helical cuts on the surface as the vibration converter. One drawback of this design is that

reversing rotor direction requires the existence of different resonance frequencies where the phase lag between the axial and torsional vibration differs by 180°. Even if this issue can be addressed, one can still expect the motor's performance to be different depending on the direction of rotation, making controlled operation more difficult.

3. DISCUSSION

Electrostatic motors were favoured by early researchers of MEMS micromotors due to their compatibility with silicon-based microfabrication techniques and the perception that they have a better force scaling characteristics ($F \propto L^1$–L^2) than the electromagnetic actuators ($F \propto L^4$) [9,43]. Various authors have noted [43,44], however, that the analysis behind the L^4 magnetic force scaling law neglects the use of permanent magnets and the increased current density that is possible as the size of magnetic actuators are decreased; given the right design a force scaling law of L^2 can be achieved (see Table 1). The scaling analyses show that electrostatic, electromagnetic and piezoelectric actuators may all have comparable force scaling characteristics of $F \propto L^2$; scaling analysis alone is insufficient for exposing an ideal choice for applications at small scales. We will thus now compare and discuss the three motor technologies in terms of their quantitative performance and their ease of miniaturization and fabrication.

3.1. Performance

In Fig. 5 the torque and power output of the motors described in the previous sections are plotted for comparison. Although the number of data point is limited, some general trends may be observed. The observed scaling laws for the three motor technologies are listed Table 3, which show that, except for ultrasonic motors, the observed trends generally falls within the range predicted by the analysis [57]; the increased index for ultrasonic motors may be due to the neglect of scaling on piezoelectric material quality in our analysis. Despite the unfavourable $\tau \propto L^4$ scaling
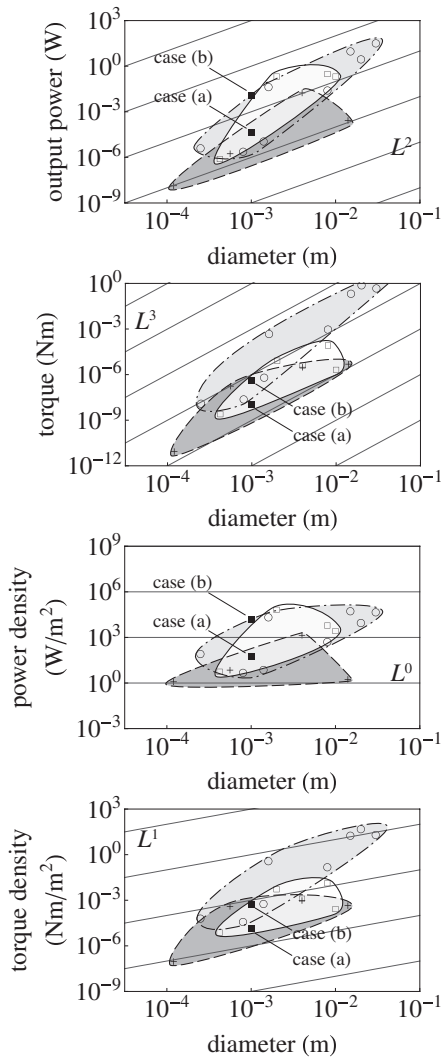
Fig. 5 Comparison of electrostatic (+), electromagnetic (□) and ultrasonic (○) motors and the performance requirements (■) of a typical future application of these motors: *endovascular micro-robots*. The regions covered by the three motor technologies are, respectively, shaded in blue, green and yellow. The following scaling laws are plotted as guides for the eyes: (a) power $\propto L^2$, (b) torque $\propto L^3$, (c) power density $\propto L^0$, and (d) torque density $\propto L^1$.

Table 3 Comparison of the observed and predicted scaling laws for electrostatic, electromagnetic and ultrasonic motors.

	Power		Torque	
	Observed	Predicted	Observed	Predicted
Electrostatic	L^2	L^{1-2}	L^3	L^{2-3}
Electromagnetic	L^4	L^{2-4}	L^3	L^{3-5}
Ultrasonic	L^3	L^2	L^4	L^3

limit of electromagnetic and ultrasonic motors. It should be noted that design details and fabrication techniques have a large influence on the motor's performance. For example, the flexural standing-wave motors of Cagatay, *et al.* [38] and Morita *et al.*'s [36] have similar diameters (1.6 and 1.4 mm respectively) but their power density have a difference of approximately four orders of magnitude.

3.2. Design and Fabrication Issues

Despite their favorable scaling characteristics, electrostatic motors generate low power and torque at the 0.1–1 mm scale. For side-drive motors, this is partly due to fabrication limitations; the torque output of electrostatic side-drive motors is proportional to the length of the stator-rotor side-wall, however, fabrication of high wall depths requires high aspect-ratio photolithography and thick resist coatings that compromises linewidth resolution. This places lower bounds on the air gap and bearing clearances that need to be minimized for high torque and low friction [11,45]. One potential solution is to use LIGA processes that can fabricate high aspect ratio structures [46]. Alternatively, efforts may be put into the miniaturization of the top-driven electrostatic induction motor [12], which has a power density of $10^3\,\mathrm{W/m^2}$ at a diameter of 4 mm. The design has the potential to compete with ultrasonic motors at scales below 0.3 mm if the scaling law of L^0 for power density can be maintained.

The difficulty of integrating magnetic materials with microfabrication is one of the chief drawbacks of electromagnetic micromotors. Various microfabrication techniques such as electroplating, sputtering, and pulsed laser deposition have been developed for magnetic materials, however, the strongest permanent magnets currently used in micromotors are still individually machined from bulk Nd-Fe-B or Sm-Co magnets [44]. Further fabrication difficulties are caused by the use of three dimensional coil-like structures in magnetic motor; solutions include the use of modified meandering coil-core structure [20], and the fabrication of coils using multiple layers of patterned conductors [26]. However, the power density of these modified designs are at least an order of magnitude lower than conventional DC brushless motors [59].

law [58], the torque generated by ultrasonic motors is about two orders of magnitude greater than the other two types of motors. At the same time, their output power is on par with electromagnetic motors. Electrostatic motors are capable of reaching the smallest diameter, however, their torque and power output are the lowest of the three motors types we have reviewed.

The power and torque requirements for micro-robot propulsion cases (a) and (b) are marked on Fig. 5 as black squares; their location relative to the performance envelopes suggest that all three motor types are capable of meeting the requirements for case (a) but not case (b); the required output power for case (b) lies just above the upper

Many of the centimeter-scale ultrasonic motors described here have very high torque and power densities, however, they are difficult to miniaturize due to fabrication issues. Most ultrasonic motor designs do not have planar geometries that are compatible with silicon-based microfabrication techniques, and designs that do use piezoelectric thin-films have poor performance due to the low electromechanical coupling coefficient [30]. For example, the circumferentially-poled transducers used in Satonobu, *et al.*'s combined axial-torsional standing wave motor (CATS motor) [39] is very difficult to fabricate at the 1–0.1 mm scale. Their construction involves cutting a piezoelectric-ceramic ring into small sectors, individually polarizing them along the circumferential direction [47], and gluing them back together. Designs that use bulk piezoelectric transducers with simple geometries and avoid complex machining are more likely to be successfully miniaturized.

The smallest ultrasonic motor reported to date, with a diameter of 0.25 mm, is a vibration-converter-type CATS motor by Watson *et al.* [41]; the motor uses a single axially-poled bulk PZT, however, its vibration converter is a hollow cylinder with helical cuts on the surface that requires the use of laser micromachining. To simplify the fabrication process of CATS micromotors, we investigate a concept proposed by Friend *et al.* [48], which is to use pretwisted beams with non-circular cross-sections as alternative vibration converters with coupled axial-torsional vibration. The vibration converter can be easily fabricated by twisting non-circular cross-section wires.

The stability problem of the early top-drive electrostatic micromotors, and the problem of friction both serves to illustrate the importance of an adequate support mechanism for the spinning rotor. Significant progress has been made over the center-pin and slide-bushing arrangements used in the early micromotors, methods such as gas bearings [13,49], microball bearings [16], and magnetic bearings [50,51] have substantially improved the performance output and the operating life of micromotors. For example, the gas bearing developed by the MIT team was capable of supporting an angular speed of up to 1.4 million rpm, with a lifetime exceeding 10^8 revolutions.

For ultrasonic motors, the stator transmits torque to the rotor via friction, thus the rotor support mechanism must serve an extra function of providing a preload to press the rotor against the stator. However, the stator-rotor interaction of CATS ultrasonic motors is not well understood; despite their high power and torque density relative to electrostatic and electromagnetic motors at the 0.1–1 mm scale, the efficiency reached by CATS ultrasonic motor is typically less than 30% [40]. The stator-rotor interface of piezoelectric motors is one of the least understood parts of the motor. Past researchers [52–54] have simplified the analysis of the interaction by assuming that the vertical position of the rotor is fixed or periodic such that the duration of contact ϕ can be determined by requiring the net vertical impulse exerted on the rotor to be zero over one stator vibration cycle, but this has been shown to be a false assumption [55]: reality is considerably more complex in these motors.

4. CONCULSIONS

A review of the electrostatic, electromagnetic and piezoelectric transduction methods for generating motion at the micro scale shows that each method offers similar scaling behavior. That is, forces generated by each method scale in a similar fashion: $F \propto L^2$. Unfortunately, and in contrast to past studies, this indicates that one cannot make a choice of which scheme to use based on scaling alone. However, piezoelectric ultrasonic transduction appears to offer far larger torque amplitudes at these small scales despite a rather unfavorable scaling law for the torque of $\tau \propto L^4$. A more serious problem is the difficulty of fabricating actuators containing high-performance piezoelectric materials, not to mention the longstanding problem of maintaining a quality contact interface as the actuator operates. The top-driven electrostatic induction motor may prove to be competitive if the support of the rotor can be properly designed for stable operation. Facing similar materials-based problems to piezoelectric motors, electromagnetic motors using permanent magnets have the advantage of over a century of development, but still suffer from poor power densities. For the time being, piezoelectric ultrasonic motors appear to offer the best potential for meeting the high performance requirements of microrobotics.

REFERENCES

[1] G. E. Moore, "Lithography and the future of Moore's law," in *SPIE*, M. H. Bennett, Ed. (SPIE, 1995), Vol. 2439, pp. 2–17.

[2] S. Paul, "Miniaturization technologies," *Tech. Rep. U.S. Congr. Off. Technol. Assess.* (1991).

[3] P. Dario, R. Valleggi, M. C. Carrozza, M. C. Montesi and M. Cocco, "Microactuators for microrobots: A critical survey," *J. Micromech. Microeng.*, **2**, 141–157 (1992).

[4] C. Li, F. E. Sauser, R. G. Azizkhan, C. H. Ahn and I. Papautsky, "Polymer flip-chip bonding of pressure sensors on a flexible Kapton film for neonatal catheters," *J. Micromech. Microeng.*, **15**, 1729–1735 (2005).

[5] S. M. Hanson, "Low voltage circuit design techniques for cubic millimeter computing," *PhD thesis, University of Michigan* (2009).

[6] B. Cook, S. Lanzisera and K. Pister, "SoC issues for RF smart dust," *Proc. IEEE*, **94**, 1177–1196 (2006).

[7] Y.-C. Tai and R. S. Muller, "Ic-processed electrostatic synchronous micromotors," *Sens. Actuators*, **20**, 49–55 (1989).

[8] R. S. Fearing, "Powering 3 dimensional microrobots: Power density limitations," *Tutorial on Micro Mechatronics and Micro Robotics, IEEE Int. Conf. Robotics and Automation* (1998).

[9] W. Trimmer, "Microrobots and micromechanical systems," *Sens. Actuators*, **19**, 267–287 (1989).

[10] S. Jacobsen, R. Price, J. Wood, T. Rytting and M. Rafaelof, "The wobble motor: Design, fabrication and testing of an eccentric-motion electrostatic microactuator," *Proc. 1989 IEEE Int. Conf. Robotics and Automation*, Vol. 3, pp. 1536–1546 (1989).

[11] M. Mehragany and Y.-C. Tai, "Surface micromachined mechanisms and micromotors," *J. Micromech. Microeng.*, **1**, 73–85 (1991).

[12] C. Livermore, A. Forte, T. Lyszczarz, S. Umans, A. Ayon and J. Lang, "A high-power MEMS electric induction motor," *J. Microelectromech. Syst.*, **13**, 465–471 (2004).

[13] L. Frechette, S. Nagle, R. Ghodssi, S. Umans, M. Schmidt and J. Lang, "An electrostatic induction micromotor supported on gas-lubricated bearings," *14th IEEE Int. Conf. Micro Electro Mechanical Systems, 2001, MEMS 2001*, pp. 290–293 (2001).

[14] M. Mehregany, S. Bart, L. Tavrow, J. Lang, S. Senturia and M. Schlecht, "A study of three microfabricated variable-capacitance motors," *Sens. Actuators A: Phys.*, **21**, 173–179 (1990), *Proc. 5th Int. Conf. Solid-State Sensors and Actuators and Eurosensors III*.

[15] M. Mehregany, S. Phillips, E. Hsu and J. Lang, "Operation of harmonic side-drive micromotors studied through gear ratio measurements," *1991 Int. Conf. Solid-State Sensors and Actuators, 1991, Dig. Tech. Pap., TRANSDUCERS '91*, pp. 59–62 (1991).

[16] N. Ghalichechian, A. Modafe, M. Beyaz and R. Ghodssi, "Design, fabrication, and characterization of a rotary micromotor supported on microball bearings," *J. Microelectromech. Syst.*, **17**, 632–642 (2008).

[17] S. F. Bart and J. H. Lang, "An analysis of electroquasistatic induction micromotors," *Sens. Actuators*, **20**, 97–106 (1989), A Special Issue Devoted to Micromechanics.

[18] S. Nagle, C. Livermore, L. Frechette, R. Ghodssi and J. Lang, "An electric induction micromotor," *J. Microelectromech. Syst.*, **14**, 1127–1143 (2005).

[19] H. Guckel, T. Christenson, K. Skrobis, T. Jung, J. Klein, K. Hartojo and I. Widjaja, "A first functional current excited planar rotational magnetic micromotor," *IEEE Micro Electro Mechanical Systems, 1993, MEMS '93, Proc. An Investigation of Micro Structures, Sensors, Actuators, Machines and Systems*, pp. 7–11 (1993).

[20] C. Ahn, Y. Kim and M. Allen, "A planar variable reluctance magnetic micromotor with fully integrated stator and coils," *J. Microelectromech. Syst.*, **2**, 165–173 (1993).

[21] H. Koser and J. Lang, "Magnetic induction micromachine — part i: Design and analysis," *J. Microelectromech. Syst.*, **15**, 415–426 (2006).

[22] D. Arnold, S. Das, F. Cros, I. Zana, M. Allen and J. Lang, "Magnetic induction machines integrated into bulk-micromachined silicon," *J. Microelectromech. Syst.*, **15**, 406–414 (2006).

[23] F. Cros, H. Koser, M. Allen and J. Lang, "Magnetic induction micromachine — part ii: Fabrication and testing," *J. Microelectromech. Syst.*, **15**, 427–439 (2006).

[24] *Namiki DC Brushless Motor SBL02-06* (Namiki Precision Jewel Co. Ltd., 2007).

[25] *Faulhaber Micro Brushless DC-Motor Series 0206 B* (Faulhaber, 2006).

[26] N. Achotte, P.-A. Gilles, O. Cugat, J. Delamare, P. Gaud and C. Dieppedale, "Planar brushless magnetic micro-motors," *J. Microelectromech. Syst.*, **15**, 1001–1014 (2006).

[27] "IEEE standard on piezoelectricity," *ANSI/IEEE Std 176-1987* (1988).

[28] T. Sashida and T. Kenjo, *An Introduction to Ultrasonic Motors* (Oxford University Press, 1993).

[29] T. Morita, "Miniature piezoelectric motors," *Sens. Actuators A: Phys.*, **103**, 291–300 (2003).

[30] J. Cho, M. Anderson, R. Richards, D. Bahr and C. Richards, "Optimization of electromechanical coupling for a thin-film PZT membrane: II. Experiment," *J. Micromech. Microeng.*, **15**, 1804–1809 (2005).

[31] T. Galante, J. Frank, J. Bernard, W. Chen, G. A. Lesieutre and G. H. Koopmann, "Design, modeling, and performance of a high force piezoelectric inchworm motor," *J. Intell. Mater. Syst. Struct.*, **10**, 962–972 (1999).

[32] J. L. Pons, *Emerging Actuator Technologies: A Micromechatronics Approach* (John Wiley & Sons, 2005).

[33] H. V. Barth, "Ultrasonic driven motor," *IBM Tech. Disclosure Bull.*, **16**, 2263–2271 (1973).

[34] V. A. e. a. Gromakovskii, "On the possibility of using a piezoelectric motor for direct actuation of the drive shaft of a video tape recorder," *Tekhnika Kino i Televideniya*, **5**, 33–43 (1978).

[35] A. M. Flynn, "Performance of ultrasonic mini-motors using design of experiments," *Smart Mater. Struct.*, **7**, 286–294 (1998).

[36] T. Morita, M. K. Kurosawa and T. Higuchi, "A cylindrical micro-ultrasonic motor (stator transducer size: 1.4 mm in diameter and 5.0 mm long)," *Ultrasonics*, **38**, 33–36 (2000).

[37] T. Kanda, A. Makino, T. Ono, K. Suzumori, T. Morita and M. K. Kurosawa, "A micro multrasonic motor using a micromachined cylinderical bulk PZT transducer," *Sens. Actuators A*, **127**, 131–138 (2006).

[38] S. Cagatay, C. Koc, P. Moses and K. Uchino, "A piezoelectric micromotor with a stator of $\phi = 1.6$ mm and $l = 4$ mm using bulk PZT," *Jpn. J. Appl. Phys.*, **43**, 1429–1433 (2004).

[39] J. Satonobu, D. Lee, K. Nakamura and S. Ueha, "Improvement of the longitudinal vibration system for the hybrid transducer ultrasonic motor," *IEEE Trans. Ultrason. Ferroelectr. Freq. Control*, **47**, 216–221 (2000).

[40] A. Suzuki and J. Tsujino, "Load characteristics of ultrasonic motors with a longitudinal-torsional converter and various nonlinear springs for inducing static pressure," *Jpn. J. Appl. Phys.*, **41**, Part 1, No. 5B, 3267–3271 (2002).

[41] B. Watson, J. Friend and L. Yeo, "Piezoelectric ultrasonic resonant motor with stator diameter less than 250 μm: The proteus motor," *J. Micromech. Microeng.*, **19**, No. 2, p. 022001 (5pp) (2009).

[42] B. Koc, S. Cagatay and K. Uchino, "A piezoelectric motor using two orthogonal bending modes of a hollow cylinder," *IEEE Trans. Ultrason. Ferroelectr. Freq. Control*, **49**, 495–500 (2002).

[43] I. J. Busch-Vishniac, "The case for magnetically driven microactuators," *Sens. Actuators A: Phys.*, **33**, 207–220 (1992).

[44] O. Cugat, J. Delamare and G. Reyne, "Magnetic microactuators and systems (magmas)," *IEEE Trans. Magn.*, **39**, 3607–3612 (2003).

[45] Z. Rymuza, "Control tribological and mechanical properties of mems surfaces. Part 1: Critical review," *Microsyst. Technol.*, **5**, 173–180 (1999).

[46] H. Guckel, "High-aspect-ratio micromachining via deep X-ray lithography," *Proc. IEEE*, **86**, 1586–1593 (1998).

[47] S. Nemoto and E. Mori, "Distribution of electric lines of force and electric field concentration in a ceramic ring to be polarized circumferentially," *Tech. Rep. Tokyo Inst. Technol.*, 123 (1974).

[48] J. Friend, K. Nakamura and S. Ueha, "Torsional transducers

using asymmetrically twisted bars with axially-poled PZT," *Proc. Spring Meet. Acoust. Soc. Jpn.*, 1-P-25, pp. 1277–1278 (2003).

[49] L. G. Frechette, S. A. Jacobson, K. S. Breuer, F. F. Ehrich, R. Ghodssi, R. Khanna, C. W. Wong, X. Zhang, M. A. Schmidt and A. H. Epstein, "Demonstration of a microfabricated high-speed turbine supported on gas bearings," *Solid-State Sensor and Actuator Workshop* (Hilton Head Is., SC, 2000), pp. 290–293.

[50] V. Fernandez, G. Reyne, O. Cugat, P.-A. Gilles and J. Delamare, "Design and modelling of permanent magnet micro-bearings," *IEEE Trans. Magn.*, **34**, 3596–3599 (1998).

[51] K. Komori and T. Yamane, "Magnetically levitated micro pm motors by two types of active magnetic bearings," *IEEE/ASME Trans. Mechatronics*, **6**, 43–49 (2001).

[52] K. Nakamura, M. Kurosawa and S. Ueha, "Characteristics of a hybrid transducer-type ultrasonic motor," *IEEE Trans. Ultrason. Ferroelectr. Freq. Control*, **38**, 188–193 (1991).

[53] K. Nakamura, M. Kurosawa and S. Ueha, "Design of a hybrid transducer type ultrasonic motor," *IEEE Trans. Ultrason. Ferroelectr. Freq. Control*, **40**, 395–400 (1993).

[54] J. Guo, S. Gong, H. Guo, X. Liu and K. Ji, "Force transfer model and characteristics of hybrid transducer type ultrasonic motors," *IEEE Trans. Ultrason. Ferroelectr. Freq. Control*, **51**, 387–395 (2004).

[55] K.-C. Liu, J. Friend and L. Yeo, "Rotating bouncing disks, tossing pizza dough, and the behavior of ultrasonic motors," *Phys. Rev. E*, **80**, No. 046201 (2009).

[56] For example, a 48 cm^3 motor by Galante, *et al.* [31], generates a stall load of 40 N and no-load speed of 6 mm/s. This implies that the force and power density are of the order of 0.8 mN/mm^3 and 5 μW/mm^3.

[57] The scaling laws for power and torque are predicted by assuming that the angular velocity ω of a micromotor is proportional to the resonance frequency of the system, which scales as L^{-1}. Thus torque scales as $\tau \propto FL$ and power scales as $P \propto \omega \propto F$.

[58] Torque is τ in this section.

[59] The power density of a conventional brushless DC motor by Faulhaber [25] with 2 mm diameter is shown on Fig. 5(c) as the peak open square point (□) in the green envelope.